

# STDP for Correlated Inputs under a Calcium-Dependent Learning Rule

**Jonathan Garcia**  
*jwgarcia@ucsd.edu*

**Akinori Mitani**  
*amitani@ucsd.edu*

**Shamit Patel**  
*ShamitPatel@ucsd.edu*

Neurosciences Graduate Program  
University of California, San Diego  
La Jolla, CA 92093

## Abstract

We used a model of spike-timing-dependent plasticity (STDP) based on calcium signaling to test the effects of correlated inputs on synaptic weight distributions. Gilson and Fukai (2011) used amplitudes for the STDP curve that depended on synaptic strength and demonstrated the emergence of stable bimodal weight distributions. Those sets of synapses with correlated inputs were more strongly potentiated than those without. However, this model did not include any biophysical mechanism for STDP. Whereas most versions of STDP model the time difference between pre- and postsynaptic spikes explicitly, as in the above study, Shouval et al (2002) used a model of NMDA-R-dependent calcium signaling to effect long-term potentiation and depression in a similar spike-timing-dependent manner to traditional STDP. We implemented a biophysical model inspired by this that used weight dependence along with modified calcium dynamics. We found that there is systematic potentiation of inputs with strong correlation, and there is depression of inputs with weak correlation.

## 1 Introduction

### 1.1 Background

Spike-timing-dependent plasticity (STDP) is a theory of learning that states that a synapse is strengthened if the presynaptic spike arrives before the postsynaptic spike, and the synapse is weakened if the presynaptic spike occurs after the postsynaptic spike [5]. We used a model of STDP based on calcium signaling to determine the effect of input correlation on synaptic weight change. Some work suggests that calcium signaling, along with other signaling mechanisms, can account for STDP [3].

### 1.2 Goals

We were interested in determining the effect of calcium signaling on long-term potentiation (LTP) and long-term depression (LTD) of synaptic strength. Our model included numerous excitatory synapses that included both AMPA and NMDA receptor kinetics along with

voltage-gated calcium channels (VGCC), all feeding into a single Hodgkin-Huxley neuron. Using different spike-timing protocols, we wanted to analyze the STDP that could result from the model. Each synapse then received a stochastic train of spikes with a given average firing rate, and different subgroups of inputs had their inputs temporally correlated at a certain frequency. With this, we wanted to test whether the correlation of input spikes could lead to distributions of potentiated and depressed synaptic weights as seen in [2].

## 2 Methodology

### 2.1 Numerical simulation

All the simulation and analysis was performed using MATLAB (Mathworks, Natick, MA, USA). The dynamics of a neuron and its synapses was modeled by differential equations which were solved numerically using Euler's method; each variable was updated every 0.05 ms based on the gradient.

### 2.2 Dynamics of a neuron

A neuron was simulated based on a Hodgkin-Huxley model. This model has four internal variables: the membrane potential  $V$ , and the three gating variables  $m$ ,  $n$ , and  $h$  representing fast  $\text{Na}^+$  channel activation, slow  $\text{Na}^+$  channel inactivation, and  $\text{K}^+$  channel activation, respectively. The dynamics of the variables are determined by the following equations:

$$\begin{aligned} \frac{dV}{dt} &= (I_{ext} + I_{Na} + I_K + I_L)/C_m , \\ I_{Na} &= g_{Na} \cdot m^3 \cdot h \cdot (E_{Na} - V) , \\ I_K &= g_K \cdot n^4 \cdot (E_K - V) , \\ I_L &= g_L \cdot (E_L - V) , \\ \frac{dm}{dt} &= \frac{0.1(V+45)}{1-\exp\left(-\frac{V+45}{10}\right)} \cdot (1 - m) - 4e^{-\frac{V+70}{18}} \cdot m , \\ \frac{dh}{dt} &= 0.07e^{-\frac{V+70}{20}} \cdot (1 - h) - \frac{1}{1+\exp\left(-\frac{V+40}{10}\right)} \cdot h , \\ \frac{dn}{dt} &= \frac{0.01(V+60)}{1-\exp\left(-\frac{V+60}{10}\right)} \cdot (1 - n) - 0.125e^{-\left(\frac{V+70}{80}\right)} \cdot n . \end{aligned}$$

$C_m = 1.0 \text{ uF/cm}^2$  is membrane capacitance,  $g_{Na} = 120.0 \text{ mS/cm}^2$  is sodium conductance,  $E_{Na} = 45.0 \text{ mV}$  is sodium reversal potential,  $g_K = 36.0 \text{ mS/cm}^2$  is potassium conductance,  $E_K = -82.0 \text{ mV}$  is potassium reversal potential,  $g_L = 0.3 \text{ mS/cm}^2$  is leak conductance, and  $E_L = -59.4 \text{ mV}$  is leak reversal potential.

### 2.3 Dynamics of synapses

Synapses were simulated using a calcium-based STDP model. Each synaptic current was fed into a neuron, and synaptic current depended on the membrane potential of the neuron.

#### 2.3.1 Receptor kinetics and calcium dynamics

Synaptic dynamics included both linear and nonlinear components. Both NMDA-Rs and VGCCs had a voltage-dependent conductance, as can be seen in Figure 1, and as described in [1]. The following variables determined the voltage-dependent fraction of channels ready for ion flux:

$$\rho_{NMDA} = \frac{1}{1 + [Mg^{++}] / 3.57 \cdot \exp(-0.062 V)} \quad (\text{for NMDA-Rs}),$$

$$\rho_{VGCC} = \frac{1}{1 + \exp(-V_{VGCC} / 7.2)} \quad (\text{for VGCCs}).$$

Because NMDA-R conductance peaks at subthreshold potentials, it is useful as a detector of excitatory postsynaptic potentials (EPSPs); because the VGCC conductance peaks at positive potentials, it acts as a detector of backpropagating action potentials (BPAPs).

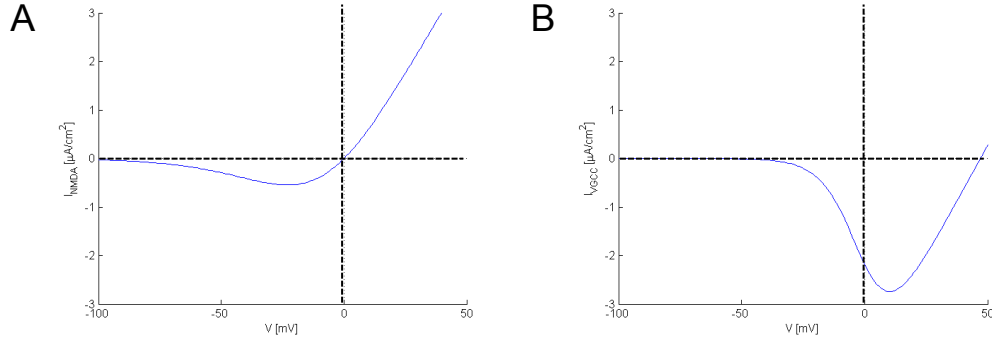


Figure 1: Current-Voltage relationships for NMDA-Rs and VGCCs. (A) Peak conductance for NMDA-Rs occurs at around -20 mV, making it a good EPSP detector. (B) Peak conductance for VGCCs occurs around +10 mV, making it a good BPAP detector.

The fraction of open glutamatergic AMPA and NMDA receptors was set to unity every time a presynaptic spike occurred, and this fraction decayed over time according to the following relationships:

$$\frac{dr_{AMPA}}{dt} = -r_{AMPA} / \tau_{AMPA} \quad ,$$

$$\frac{dr_{NMDA}}{dt} = -r_{NMDA} / \tau_{NMDA} \quad ,$$

with  $\tau_{AMPA} = 2.5$  ms and  $\tau_{NMDA} = 30$  ms.

$V$  is the membrane potential of the spine, and it receives currents from the neuroreceptors, from the calcium channels, from the soma (to mediate BPAPs), and from leakage. The dynamics of the variables are determined by the following equations:

$$I_{soma} = g_{fb} \cdot (V_{soma} - V) \quad ,$$

$$I_{AMPA} = g_{AMPA} \cdot r_{ampa} \cdot (E_{AMPA} - V),$$

$$I_{NMDA} = g_{NMDA} \cdot \rho_{NMDA} \cdot r_{NMDA} \cdot (E_{NMDA} - V) \quad ,$$

$$I_{VGCC} = g_{VGCC} \cdot \rho_{VGCC} \cdot (E_{Ca} - V_{VGCC}) \quad ,$$

$$I_L = g_L \cdot (E_L - V) \quad , \quad (\text{leak term})$$

$$\frac{dV}{dt} = (I_{soma} + I_{AMPA} + I_{NMDA} + I_{VGCC} + I_L) / C_m \quad .$$

For the model to work, a nonlinearity had to be introduced to the VGCCs, namely that the voltage they experienced was equal not to the synaptic membrane voltage, but to the sum of the membrane voltage with an extra voltage term from the NMDA-R activity, according to the following equations:

$$\frac{dV_{NMDA}}{dt} = 30 I_{NMDA}/C_m - V_{NMDA}/\tau_{NMDA} ,$$

$$V_{VGCC} = V + V_{NMDA}.$$

The effects of adding this can be seen in Figure 3B. Biophysically, this might represent the VGCCs being located close to the NMDA-Rs in the postsynaptic membrane, allowing them to feel an extra local voltage increase following presynaptic activity. Finally, calcium influx occurred both through NMDA-Rs and through VGCCs, decaying toward a basal concentration of zero without any activity:

$$\frac{d[Ca^{++}]}{dt} = (I_{NMDA} + I_{VGCC}) - [Ca^{++}]/\tau_{Ca}$$

The level of calcium in the synaptic spine compartments determined how the synaptic strength would change.

### 2.3.2 Spike-timing dependent plasticity

Spike-timing dependent plasticity (STDP) changes synaptic strength through the inclusion or removal of AMPA-Rs [4]. We simulated this by having synaptic strength change through the updating of  $g_{AMPA}$ , using a learning rule that depends on the level of calcium in the synaptic spine alone [2][5]. The following system of equations describes the update rule:

$$D_{rate} = -g_{AMPA} \quad (\text{depression rate}),$$

$$P_{rate} = 2 e^{-(g_{AMPA})^2} \quad (\text{potentiation rate}),$$

$$\theta_D = 0.215g_{AMPA} + 0.895 \quad (\text{depression threshold}),$$

$$\theta_P = -1.363g_{AMPA} + 2.626 \quad (\text{potentiation threshold}),$$

$$\omega = D_{rate} \cdot H([Ca^{++}] - \theta_D) + P_{rate} \cdot H([Ca^{++}] - \theta_P),$$

$$\eta = \frac{1}{1 + \exp(-5 \cdot ([Ca^{++}] - 0.5))} \quad (\text{learning rate}),$$

$$\frac{dg_{AMPA}}{dt} = \eta \cdot \omega / \tau_{STDP} \quad (\text{weight update}).$$

The depression and potentiation rates limit how quickly each of the independent LTD and LTP mechanisms operate, respectively, and the thresholds ensure that each of these occur at only a certain level of  $[Ca^{++}]$ . The learning rate ensures that strong weight changes occur only after large calcium influxes.

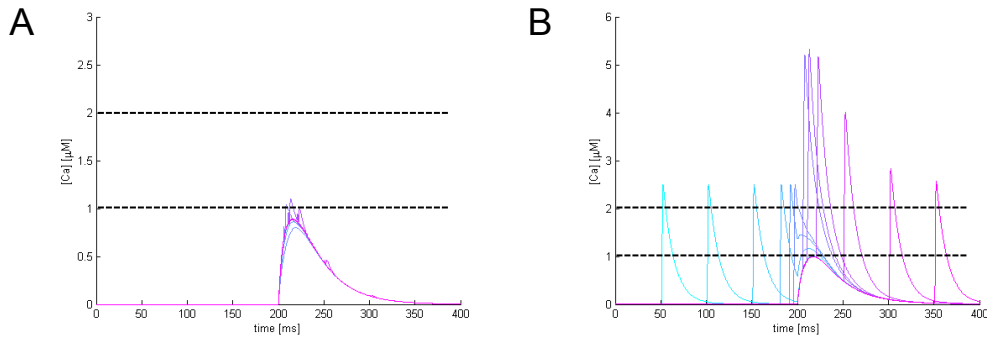


Figure 2: VGCCs are crucial for calcium-based STDP;  $\Delta t = t_{post} - t_{pre}$  shown between -150 and +150 ms, centered on presynaptic EPSP. Approximate potentiation (top line) and depression (bottom line) thresholds are depicted (A) With no VGCCs, BPAPs are not visible at all except after a presynaptic input, when the NMDA-Rs open from neurotransmitter release; there is virtually no distinction in  $[Ca^{++}]$  for causal or anti-causal activity. (B) Addition of VGCCs provide clear distinction between EPSPs and BPAPs, as well as excellent causal/anti-causal distinction in calcium levels.

The synapse should depress whenever a BPAP precedes an EPSP, representing anti-causal activity, and it should potentiate whenever an EPSP precedes a BPAP, representing causal activity. For this to work, each of the relative timings must produce distinct profiles in the calcium transients generated. The supplementary information of Graupner and Brunel’s paper [3] shows a model (G-B) for implementing STDP with calcium thresholds for LTD and LTP that uses explicit timing information of the BPAP and EPSP. We compared our model to theirs and adjusted the conductances and time constants of the NMDA-Rs and VGCCs in our model until our calcium dynamics nearly matched theirs for different timing protocols, as seen in Figure 3. Our model is more biophysical in this regard in that it uses only simulated ion channels to achieve the desired calcium profiles.

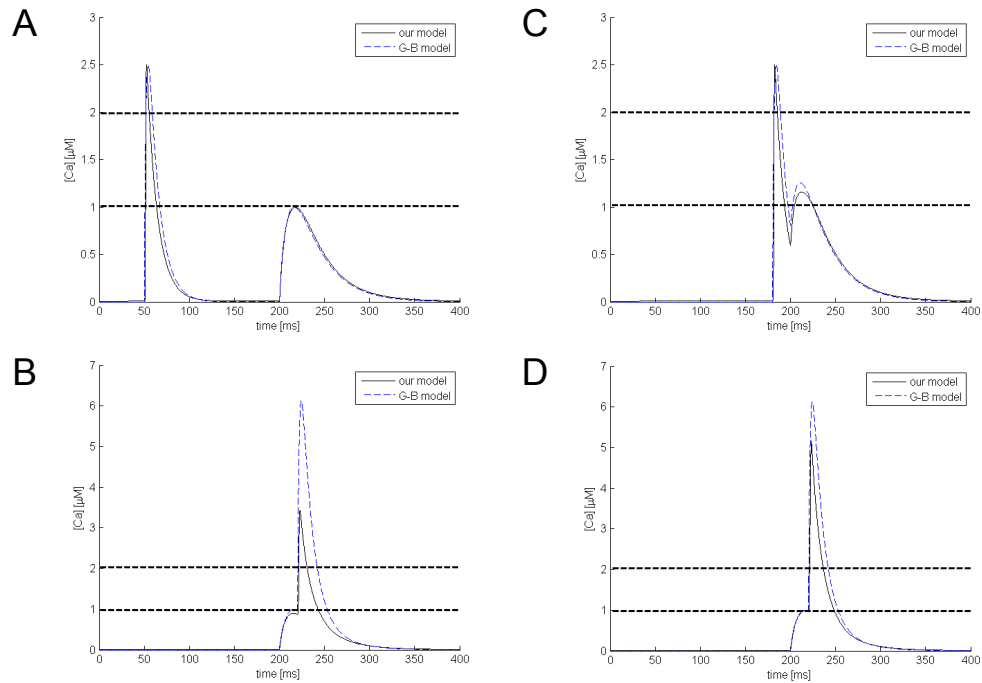


Figure 3: Calcium dynamics of our model compared to the Graupner-Brunel (2012) model with approximate potentiation (top line) and depression (bottom line) thresholds depicted. (A) Calcium transient from postsynaptic BPAP (mediated by VGCCs) followed 150 ms later by calcium transient from presynaptic EPSP (mediated by NMDA-Rs). (B) Summing of calcium at  $\Delta t = t_{\text{post}} - t_{\text{pre}} = +20$  ms before nonlinear component introduced to our model; too little time is spent in LTP region. (C) Summing of calcium at  $\Delta t = -20$  ms; most time is spent in LTD region. (D) Summing of calcium at  $\Delta t = +20$  ms after introduction of nonlinear component; more time is spent in LTP region.

We test our model in later sections.

## 2.4 Correlated inputs

Beyond simply achieving biophysically implemented STDP, we wanted to test the effects of having inputs temporally correlated, on the LTP and LTD of synapses. We inputted spike trains to 80 simulated synapses, using the model described above, using different forms of correlation: full, sinusoidal, and none (see Figure 4).

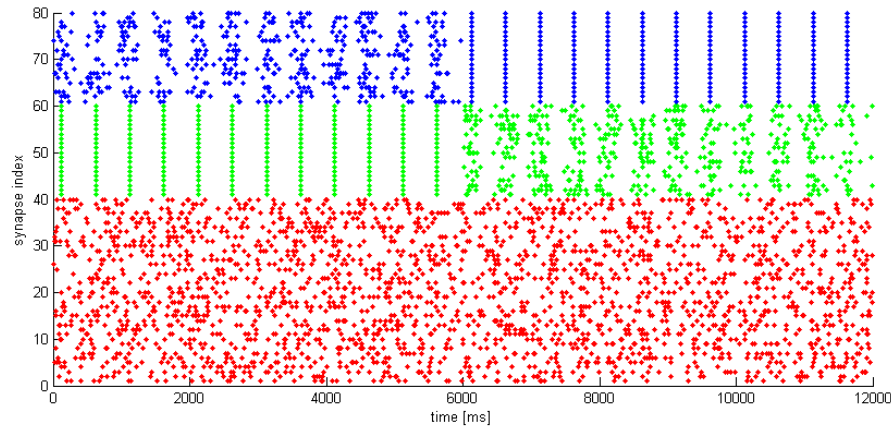


Figure 4: Spike trains for 80 synaptic inputs to the model, showing sinusoidal correlation (top/blue for first 6 seconds, middle/green for last 6 seconds), full correlation (middle/green for first 6 seconds, top/blue for last 6 seconds), or no correlation (red/bottom).

Average firing frequency: 5 Hz. Correlation frequency: 2 Hz.

Receiving these inputs over a period of 12 seconds of simulation time, we observed the changes in the synaptic weight distribution.

### 3 Results

#### 3.1 LTP and LTD: dependent on timing, weight, and frequency

As you can see in Figure 5 on the next page, as we hoped, as the synaptic weight increases, LTP decreases and LTD increases. This results in saturation of the synapse [2]. In our STDP rule, we didn't use any hard upper bounds on the weight, as some models do. Instead, like in [2], we used a weight-dependent decrease in potentiation and a weight-dependent increase in depression that kept the weight from diverging to infinity during LTP. When we take away the VGCC's, STDP is eliminated, showing that good models of STDP need to take these into account in addition to the NMDA-Rs. This contrasts with [5], which didn't get a standard STDP curve because they didn't take into account the other calcium channels.

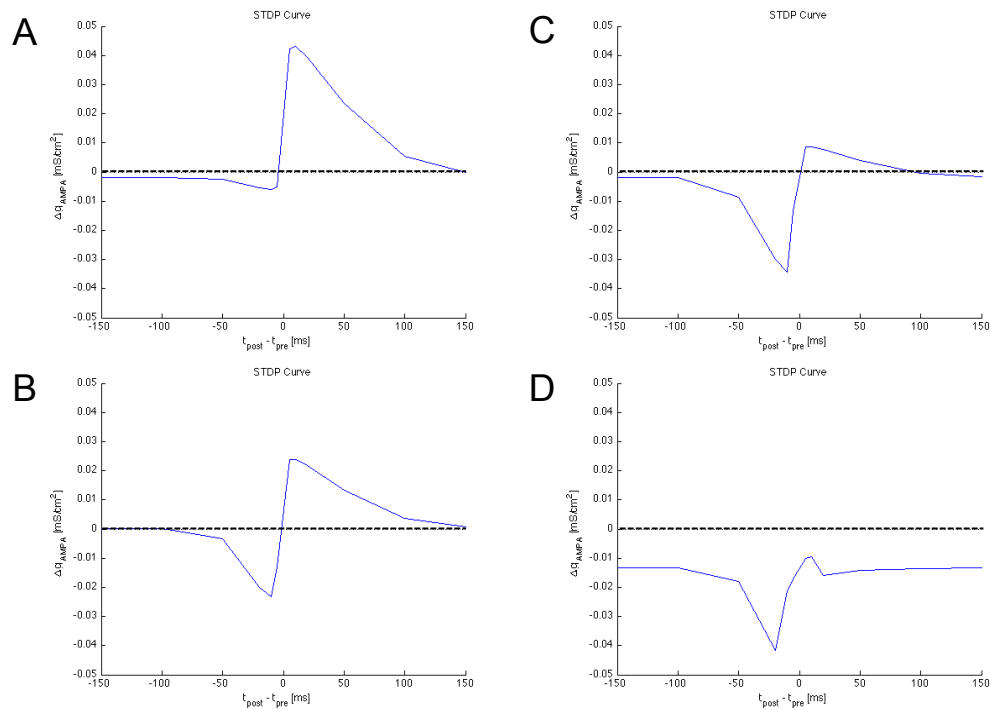


Figure 5: STDP curves at different initial weights; depression can be seen in anti-causal region ( $t_{\text{post}} - t_{\text{pre}} < 0$ ); potentiation is seen in causal region ( $t_{\text{post}} - t_{\text{pre}} > 0$ ). (A) LTP outweighs LTD for small initial weight of  $0.1 \text{ mS/cm}^2$ . (B) Nearly equal potentiation and depression for moderate initial weight of  $0.5 \text{ mS/cm}^2$ . (C) LTD outweighs LTP for large initial weight of  $0.7 \text{ mS/cm}^2$ . (D) At large weights ( $0.9 \text{ mS/cm}^2$  in figure), learning rule becomes all depression.

Figure 6, on the next page, shows frequency response curves for various initial weight values. A frequency response curve shows how LTP and LTD can depend on input frequency alone. Figure 6B shows what electrophysiologists would typically see, but at low frequencies, we see LTD, and at high frequencies, we see LTP. Nevertheless, as you can see in Figure 6A, for low weights, slight LTD occurs at all stimulation frequencies. Also, as can be seen in Figure 6D, for very high weights, LTD occurs at all frequencies. Finally, as you can see in Figure 6C, for moderate weights, LTP occurs at all frequencies.

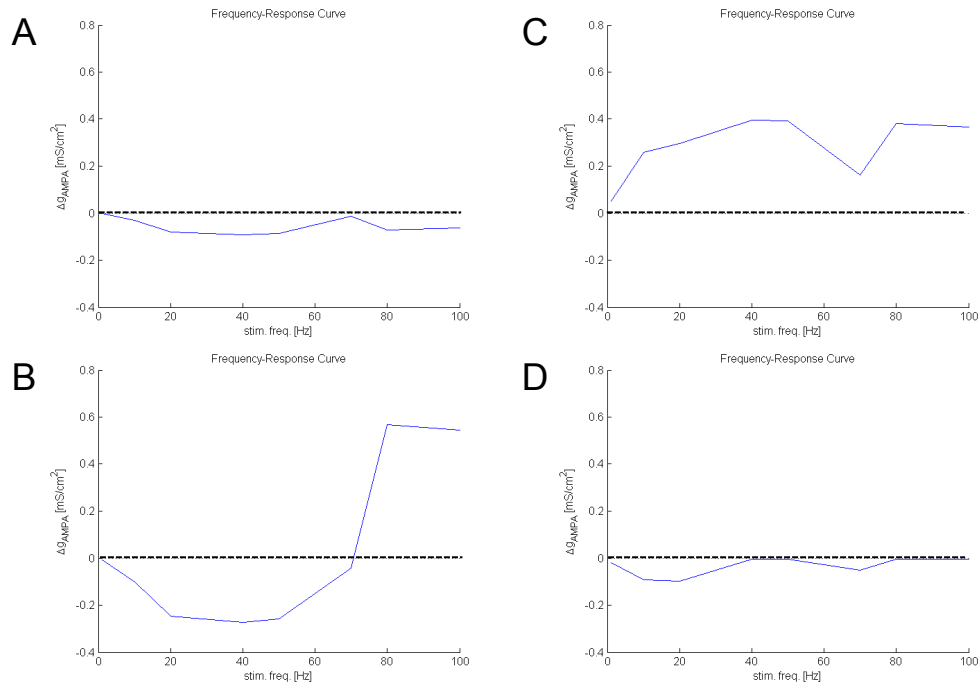


Figure 6: Frequency response curves for different initial weight values on a neuron of moderate excitability. (A) At  $0.1 \text{ mS/cm}^2$ , slight depression occurs at all stimulation frequencies. (B) At  $0.3 \text{ mS/cm}^2$ , depression region occurs for small to moderate stimulation frequencies, and saturating potentiation occurs for high stimulation frequencies. (C) At  $0.5 \text{ mS/cm}^2$ , every stimulation drives postsynaptic output, so all frequencies see LTP. (D) At  $0.9 \text{ mS/cm}^2$ , all-depression learning rule takes over, and all stimulation frequencies cause LTD.

### 3.2 Model output given input spike trains

Figure 7A on the next page shows the postsynaptic spikes that were driven at each instance of correlated input. Initial weights too small to elicit postsynaptic spikes saw only depression on other runs. Figure 7B shows the response of the model to the inputs given in Figure 4. As you can see, fully correlated inputs showed LTP that saturated without any upper limit. Also, sinusoidally correlated inputs exhibited both LTP and LTD. Finally, inputs that were completely uncorrelated demonstrated LTD exclusively. All of these results were what we expected, so we can conclude that full input correlation yields LTP, while full input decorrelation yields LTD.

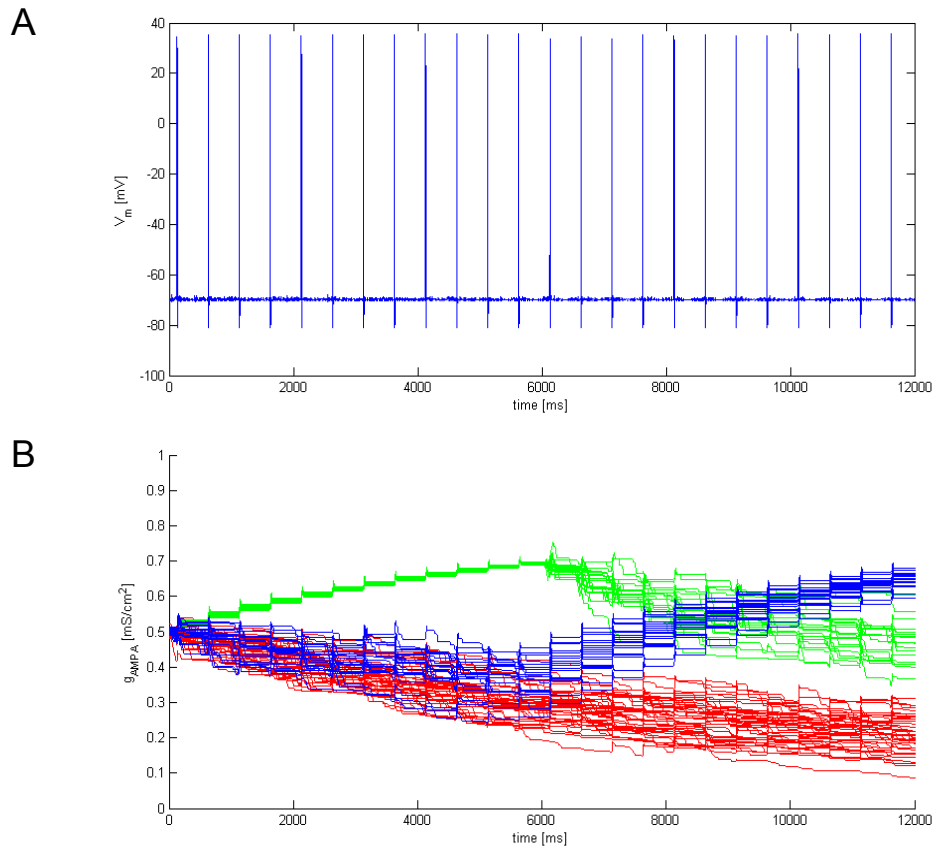


Figure 7: Response of model to inputs given in Figure 4. (A) Postsynaptic spikes were driven at each instance of correlated input; initial weights too small to elicit post-synaptic spikes saw only depression on other runs (not shown). (B) Changes in synaptic weights. Inputs that were fully correlated (green for first six seconds, blue for last six seconds) exhibited LTP that saturated without any explicit upper bound. Inputs with sinusoidal correlation (blue for first six seconds, green for last six seconds) showed slightly less tendency to depress than those completely uncorrelated (red), whose weights stochastically decayed.

## 4 Conclusions

We showed, using a model of STDP based on calcium signaling, that as expected, fully correlated inputs exhibit LTP, while fully decorrelated inputs show LTD. We also demonstrated that as synaptic weight increases, LTP decreases and LTD increases. This results in saturation of the synapse [2]. We also showed that at low stimulation frequencies, we see LTD, and at high frequencies, we see LTP. Together, these results may help us better understand how learning occurs in the brain because of the biophysically realistic model on which they are based.

## References

- [1] Almog, M., & Korngreen, A. (2009). Characterization of voltage-gated  $\text{Ca}^{2+}$  conductances in layer 5 neocortical pyramidal neurons from rats. *PLoS ONE*, 4(4), 1-11. doi:10.1371/journal.pone.0004841
- [2] Gilson, M., & Fukai, T. (2011). Stability versus neuronal specialization for STDP: Long-tail weight distributions solve the dilemma. *PLoS ONE*, 6(10), 1-18. doi:10.1371/journal.pone.0025339
- [3] Graupner, M., & Brunel, N. (2012). Calcium-based plasticity model explains sensitivity of synaptic changes to spike pattern, rate, and dendritic location. *PNAS*, pp. 1-6. doi:10.1073/pnas.1109359109
- [4] Malinow, R. (2003). AMPA receptor trafficking and long-term potentiation. *Philos Trans R Soc Lond B Biol Sci.*, 358(1432), 707-714. doi:10.1098/rstb.2002.1233
- [5] Shouval, H. Z., Bear, M. F., & Cooper, L. N. (2002). A unified model of NMDA receptor-dependent bidirectional synaptic plasticity. *PNAS*, 99(16), pp. 10831-10836. doi:10.1073/pnas.152343099